Journal of Advanced Research in Natural and Applied Sciences
dergipark.org.tr/en/pub/jarnas
Open Access

ISSN: 2757-5195 11 (3) (2025) 260-275 doi.org/10.28979/jarnas.1704353

An Investigation into the Liquefaction Phenomena in the Iskenderun Bay Following the February 6 Kahramanmaraş Earthquake

Yusuf Güzel[1], Fidan Güzel[2]

Article Info
Received: 22 May 2025
Accepted: 11 Jun 2025
Published: 30 Sep 2025
Research Article

Abstract − This study investigates the liquefaction phenomena in the İskenderun Bay by revisiting the site that was liquefied during the first major strike of the Kahramanmaraş earthquake events on February 6th, 2023 (with a moment magnitude of 7.7). Firstly, the recorded input motions around the site are described. Accordingly, the soil profiles at the site are illustrated, along with the measured Standard Penetration Test (SPT) values. Later, the liquefaction analyses are conducted using a simplified method. Additionally, the two soil profiles are modelled and simulated under one of the recorded input motions at the site. Both analytical and numerical results clearly illustrate a high level of liquefaction possibility, with safety factors well below the threshold value of 1, particularly at the granular soil layers. Moreover, the generation of excess pore water pressure appears to increase as it moves through the ground surface within the sandy and silty soil layers. This implicitly indicates the liquefaction susceptibility of granular soil layers at the top 20 m of the site. It also highlights the effectiveness of the simplified and numerical approaches in predicting liquefaction.

Keywords *– Kahramanmaraş earthquake event, liquefaction, simplified approach, numerical approach, excess pore water pressure*

1. Introduction

Soil liquefaction remains a critical concern in seismic regions, particularly for loose, saturated sandy, and silty soils. It is a seismic phenomenon that occurs when saturated soil loses its strength due to an increase in pore water pressure, causing it to behave like a viscous fluid. This loss of soil strength occurs when cyclic loading, such as that caused by earthquakes, builds up excessive pore water pressure, reducing the effective stress to near zero [1]. Liquefaction susceptibility is particularly high in seismically active regions, where earthquake-induced motions often trigger it. Assessing liquefaction risk is critical for infrastructure protection, seismic hazard evaluation, and urban planning [2, 3].

Liquefaction can have devastating consequences, including foundation failure, lateral spreading, road subsidence, and the upheaval of buried pipeline systems, often due to phenomena such as sand boiling and soil settlement [4]. Historical examples of liquefaction-induced damage include major earthquakes, such as the 1964 Good Friday earthquake in Alaska and the Niigata earthquake in Japan [5-8]. More recent examples include the 1992 Erzincan earthquake [9], the 1998 Adana-Ceyhan earthquake [10], the 1999 Izmit (Kocaeli) earthquake [11], the 2010 Christchurch earthquake [12, 13], and the 2018 Indonesia earthquake [14].

The recent Kahramanmaraş earthquakes serve as a reminder of the devastating impact liquefaction on infrastructure and communities. In particular, on February 6th, 2023, the Kahramanmaraş region in southern

[1]yusufkurtdereli@hotmail.com (Corresponding Author); [2]xyfidanozdemir@hotmail.com
[1,2]Department of Civil Engineering, Faculty of Engineering, Iğdır University, Iğdır, Türkiye

Türkiye was struck by a devastating magnitude 7.7 earthquake, followed by a 6.7 magnitude aftershock approximately ten minutes later, and a third, 7.6 magnitude event occurred nine hours later [15, 16]. These seismic events led to widespread destruction, affecting an estimated 14 million people. The earthquake sequence resulted in extensive damage, primarily due to the strong inertial forces that destroyed entire villages and towns [17-19]. Liquefaction was a contributing factor in some of these areas, leading to the lateral spreading near rivers and shorelines, extreme settlement, and tilting of structures, often without significant structural damage [20, 21]. Liquefaction-induced damage differs from other forms of destruction, as it results from the rapid buildup of pore pressure in loose, saturated soils, causing the loss of the foundation capacity of buildings or, in extreme cases, causing the soil beneath structures to liquefy completely, leading to partial subsidence [22, 23]. Additionally, liquefaction can cause buried structures to rise to the surface [18]. The city of Iskenderun, and especially Gölbaşı, experienced significant liquefaction during the February 6th earthquake sequence. This led to extensive damage to its structures and infrastructure, as reported by Yıldız et al. [24] and Çetin et al. [25].

Evaluating the potential for liquefaction initiation is crucial when soil deposits are prone to liquefaction. Among the most commonly used methods in geotechnical engineering practice is the simplified procedure by Seed and Idriss [26], which employs cyclic shear stress (CSR) to assess ground motion during earthquakes. This method compares CSR to the cyclic shear strength ratio (CRR). It determines CRR values using data from standard penetration tests (SPT) and Cone Penetration Tests (CPT) [27]. One-dimensional (1D) site response analysis is another commonly used method to study how local soil conditions affect seismic wave propagation [28, 29]. It has become a standard technique in geotechnical engineering, employing various methods, including linear, equivalent linear, and nonlinear analyses. Linear analysis can be performed in both the frequency and time domains, with equivalent linear analysis in the frequency domain and nonlinear analysis in the time domain [30, 31]. The primary distinction between these methods is their treatment of shear strain. Linear and equivalent linear methods assume that damping and shear modulus are independent of shear strain, while nonlinear analysis considers strain dependency [32, 33].

This study aims to predict the liquefaction case observed during the first main Kahramanmaraş earthquake event in a site close to the city of Iskenderun (close to the Iskenderun Bay as liquefaction cases are presented in Figures 1 and 2 [21]). 11 boreholes drilled around the Iskenderun Bay near the liquefaction case are taken into consideration. Simplified and nonlinear numerical methods are utilized to assess the liquefaction potential at the site. The recorded input motion from the earthquake event recorded at the stiff soil site is used. The paper continues by describing the seismicity of the area and the recorded input motions within the city of Iskenderun. Later, it gives information about the site by featuring the soil layers at the considered boreholes. Subsequently, the simplified liquefaction assessment method is described along with the presentation of factors of safety against liquefaction. Lastly, the numerical method is outlined, and its results, in terms of the excess pore water ratio, are presented.

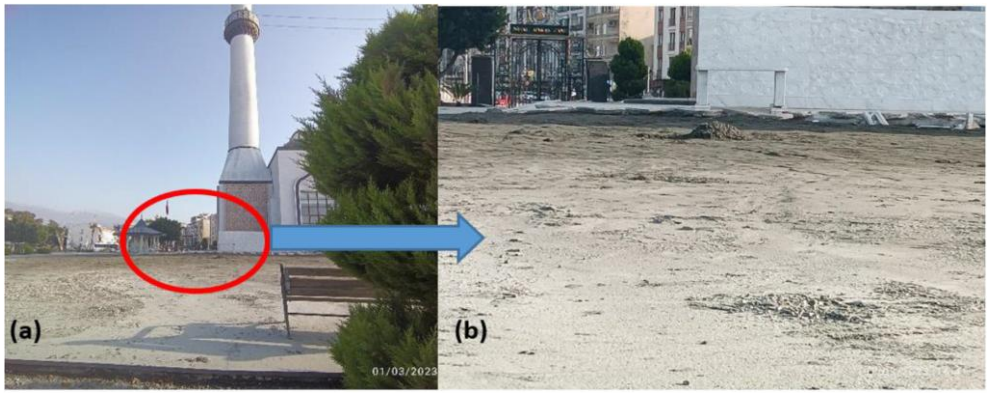

Figure 1. Surface ejecta observed around the close to İskenderun Bay during the first main Kahramanmaraş earthquake event

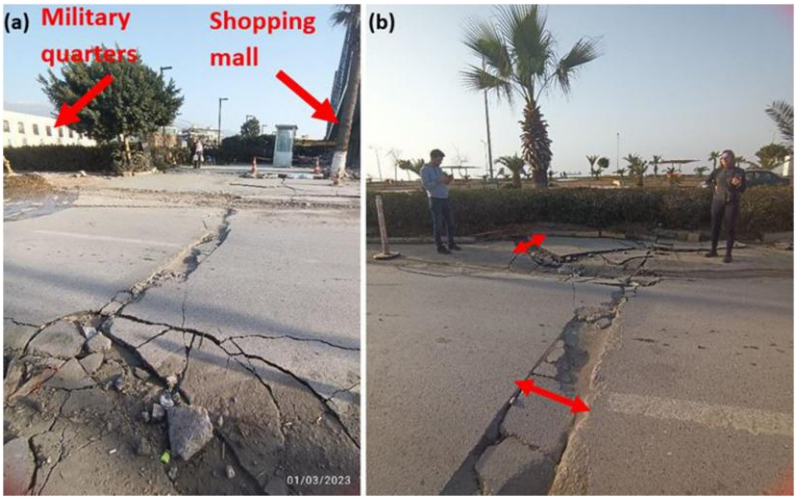

Figure 2. Liquefaction-linked damages observed around the Iskenderun Bay during the first main Kahramanmaraş earthquake event

2. Recorded Input Motions from the First Main Kahramanmaraş Earthquake Event

Türkiye has been equipped with several accelerometers throughout the country, particularly in the high-seismic potential regions. The city of Iskenderun is one of the regions affected due to its proximity to the East Anatolian Fault Zone (EAFZ), which passes through Hatay city. Figures 3a and 3b represent the peak ground acceleration (PGA) distributions over Türkiye, as suggested by the Disaster and Emergency Management Presidency (AFAD), and specifically within and around Iskenderun city, respectively. It is evident that the sites near the EAFZ and North Anatolian Fault Zone (NAFZ) exhibit the highest PGA levels, reaching a value of 0.76g [34]. The far the sites get from the fault zones, the less the PGA intensity becomes (as seen in Figure 3a). For the particularly interested Iskenderun area, the PGA ranges from 0.31g to 0.40g, as shown in Figure 3b.

Table 1. Details of the first main Kahramanmaraş earthquake event

Event ID	Event Date	Agency	Lon.	Lat.	Type	Magnitude	Depth	Location
543428	06/02/2023 04:17	AFAD	37.043	37.288	M_w	7.7	8.6	Pazarcık (Kahramanmaraş)

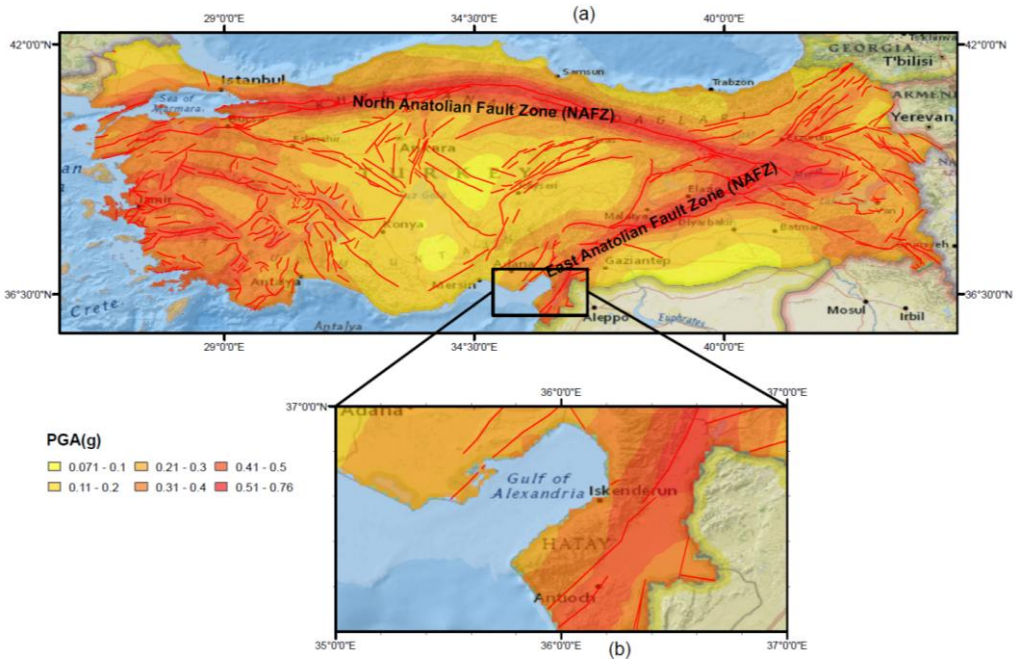

Figure 3. (a) PGA distributions over the country of Türkiye and (b) around the area of interest (i.e., the city of Iskenderun) provided by AFAD to be considered in seismic design of structures

Within Iskenderun city, 10 earthquake stations were installed. However, at only two stations, the full recordings of the seismic waves from the first main Kahramanmaraş earthquake event were recorded. The properties of the earthquake event and those of these two stations are presented in Tables 1 and 2, respectively, and illustrated in Figure 4. While station #3116 is positioned on a site with soil class A, station #3115 is located on a relatively soft site with a soil class of B, according to the Eurocode 8 (EC8) soil classification scheme. The shear wave velocities at the top 30 m $(V_{S,30})$ are 870 m/s and 424 m/s, respectively, on average for the sites.

Table 2. Properties of stations #3116 and #3115 and PGA values of the recorded input motions in EW and NS directions

Station code	longitude	Latitude	$V_{S,30}$ (m/s)	PGA in EW (in unit g)	PGA in NS (in unit g)
3116	36.20661	36.61618	870	0.168	0.149
3115	36.1646	36.54634	424	0.226	0.290

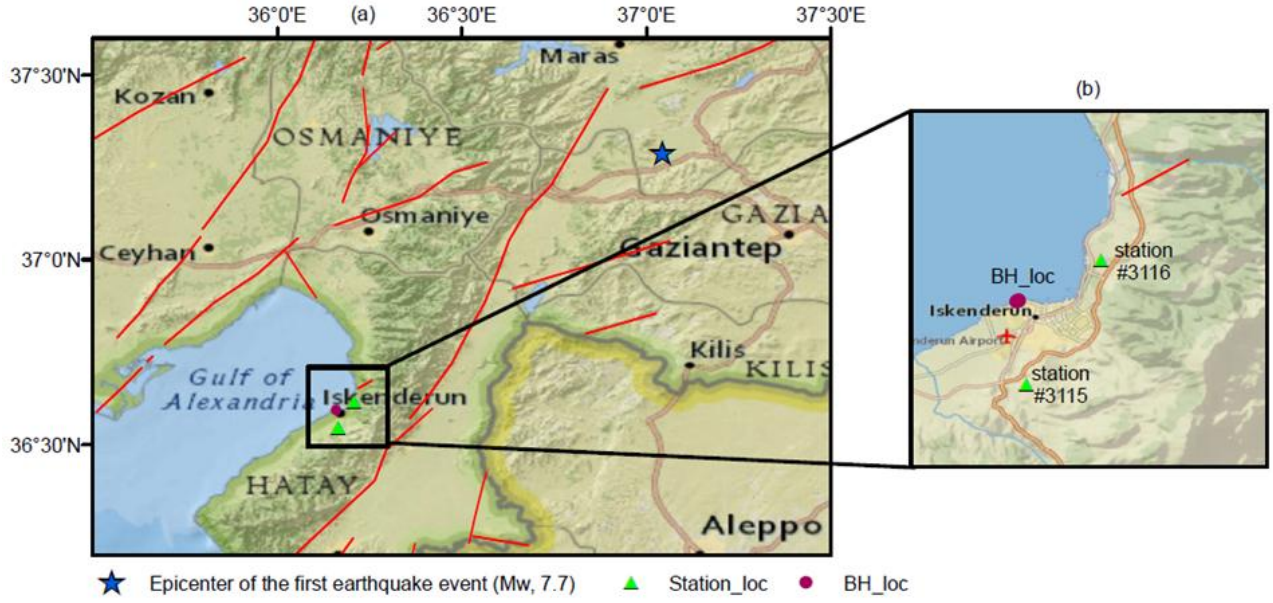

Figure 4. Epicenter of the first main Kahramanmaraş earthquake event and the locations of stations #3116 and #3115 and the geotechnical boreholes in wider (a) and narrower (b) perspectives

The recorded input motions in the East-West (EW) and North-South (NS) directions are illustrated in Figure 5. The epicentral distance is 105.38 km for station #3116, while it is 113.57 km for station #3115. The PGA values of the input motions recorded at station #3116, located at the stiff site, are lower than those recorded at station #3115. More precisely, the PGA values at station #3116 are 0.168g and 0.149g in the EW and NS directions, respectively. Accordingly, these values are equal to 0.226g and 0.29g at the station #3115. It is obvious that the PGA values at the relatively soft site are greater than those recorded at the stiff site. This can directly be attributed to the site effect. Since seismic energy is transferred to longer periods, the input motion tends to amplify as well [35-37]. In this study, the recorded input motion in the EW direction at the stiff site (i.e., outcrop input motion) is utilized for simplified and numerical liquefaction analyses.

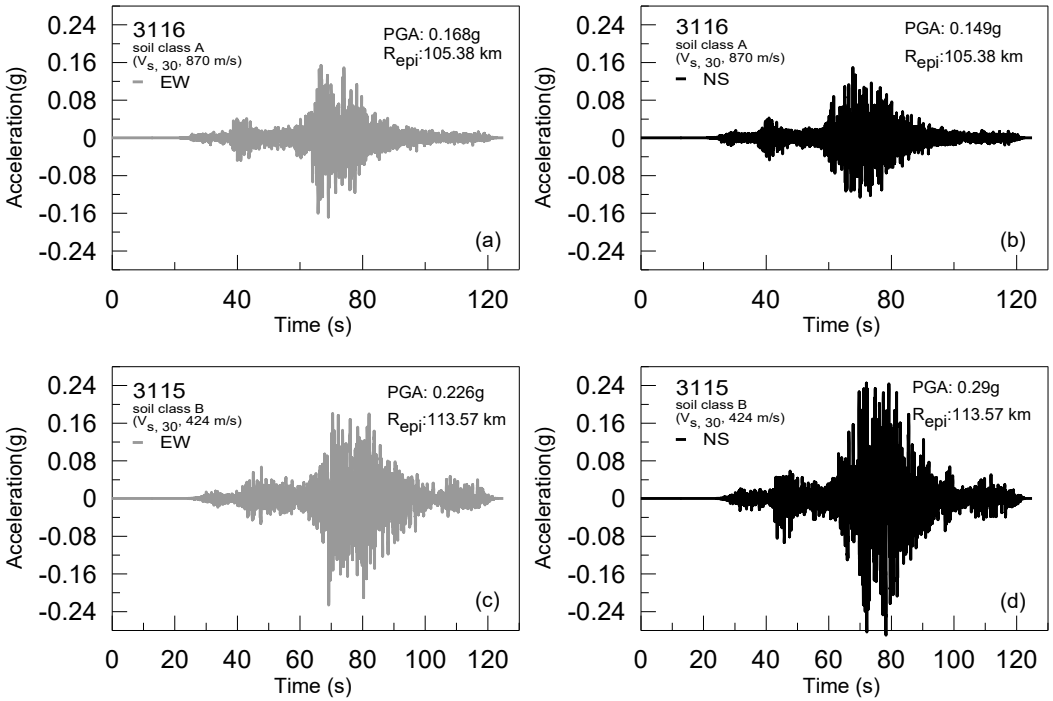

Figure 5. Acceleration-time histories of the recorded input motions from the first main Kahramanmaraş earthquake event at stations 3116 and #3115 in the EW and NS directions of the site

3. Geotechnical Characteristics of the Site and Simplified Liquefaction Analysis

3.1. Geotechnical Data

The area of interest is close to the Iskenderun Bay. The characterization of the site is based on 11 drilled boreholes. The boreholes are located in the soil deposits around the Iskenderun Bay, as reported in the study by Ozener et al. [21]. The classified soil layers, along with the corrected SPT-N ($N_{1,60}$) profiles, are provided in Figures 6-8. The boreholes are generally drilled at depths above 40 m, ranging from as low as 39 m to as high as 46 m. The site primarily consists of silt and sand soil layers, particularly at the top 20 m, and is interlayered with clay and silt soil layers (and in several boreholes, sand soil layers) between approximately 20 m and 40 m in depth. In addition, the clay soil layer is encountered at the depths of 40 to 50 m, which is underlain by sandstone. The $N_{1,60}$ values are generally greater than 12 at the top 10 m but hover mainly around 8 to 12 in most of the boreholes.

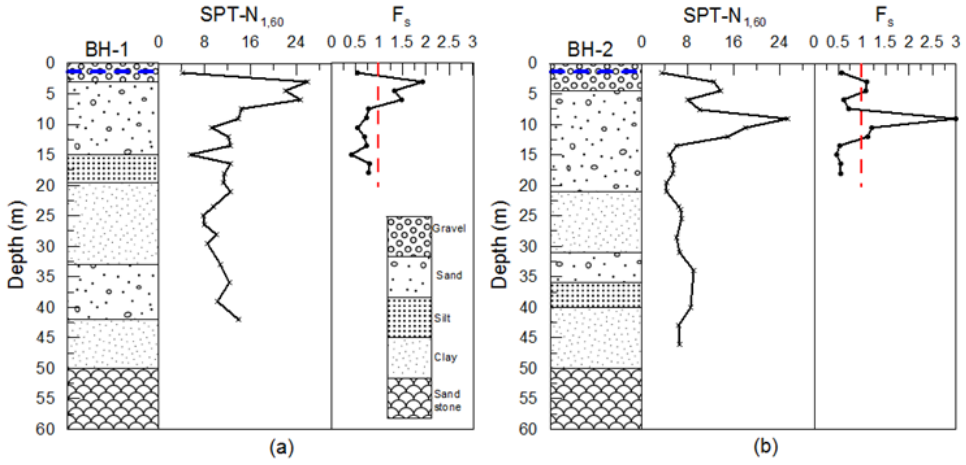

Figure 6. Soil layers at the BH-1, BH-2, BH-3, and BH-4 and corresponding corrected SPT-N values $(N_{1,60})$ and factors of safety (F_S) against liquefaction

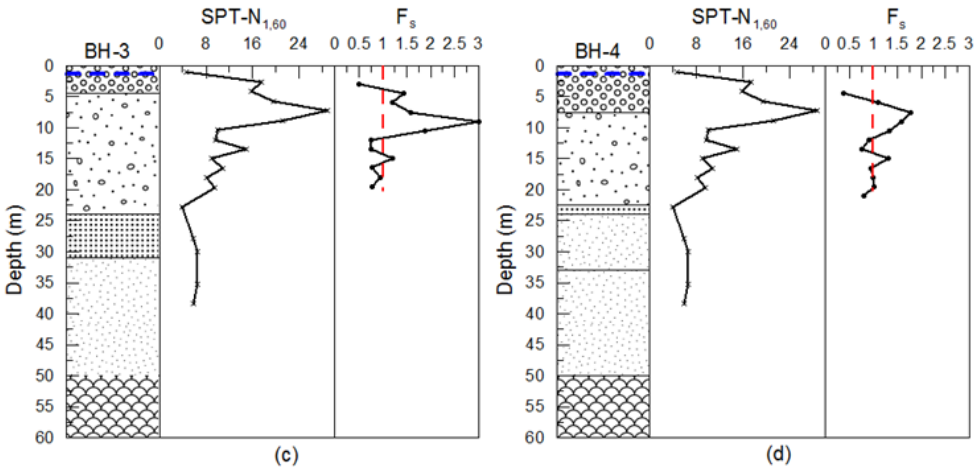

Figure 6. (Continued) Soil layers at the BH-1, BH-2, BH-3, and BH-4 and corresponding corrected SPT-N values $(N_{1,60})$ and factors of safety (F_S) against liquefaction

3.2. Results of Simplified Liquefaction Analysis

The widely recognized simplified SPT-based method proposed by Seed and Idriss [26] and later refined by Seed et al. [38] is used. The correction of the N_{30} values is performed using the equation provided by Youd and Idriss [39] below.

$$(N_1)_{60} = N_m C_N C_E C_B C_R C_S \tag{3.1}$$

In this context, N_m represents the measured standard penetration counts, C_N is the normalization of N_m relative to the reference overburden pressure in non-cohesive soils, C_E is the hammer's energy efficiency level, C_B is the correction factor dependent on the radius of a rod, C_R The correction factor is dependent on rod length, and CS represents the correction for the borehole sampler. The correction factor C_N is calculated using the equation proposed by Liao and Whitman [40].

$$C_N = \left(\frac{P_a}{\sigma'_{vo}}\right)^{0.5} \tag{3.2}$$

Here, P_a refers to the atmospheric pressure, approximately 100 kPa, and σ'_{vo} represents the effective overburden pressure, which cannot exceed 1.70. Additionally, since the fine content in clean sand is known to affect the soil's liquefaction resistance, corrections based on fine content (FC) are recommended.

$$(N_1)_{60cs} = \alpha + \beta (N_1)_{60} \tag{3.3}$$

In this case, α and β coefficients are determined on the level of fine content inclusions, as follows:

$$FC \leq 5\%, \alpha = 0, \text{and } \beta = 1$$

$$5\% < FC \leq 35\%, \alpha = \exp\left[1.76 - \frac{190}{FC^2}\right], \text{ and } \beta = \left[0.99 + \frac{FC^{1.5}}{1000}\right] \tag{3.4}$$

$$FC \geq 35\%, \alpha = 5, \text{and } \beta = 1.2$$

To assess the liquefaction potential of soil, it is essential to calculate the cyclic resistance ratio (CRR) and cyclic stress ratio (CSR). The CRR represents the soil's resistance to liquefaction, while the CSR indicates the level of shear stress within the soil during a potential earthquake. The formulas for calculating both CRR and CSR were initially provided by Seed et al. [38] using the following equations:

$$CRR_{7.5} = \frac{1}{34 - (N_1)_{60}} + \frac{(N_1)_{60}}{135} + \frac{50}{[10(N_1)_{60} + 45]^2} - \frac{1}{200} \tag{3.5}$$

$$CSR = 0.65 \frac{\alpha_{\max}}{g} \frac{\sigma_{vo}}{\sigma'_{vo}} r_d \tag{3.6}$$

In this context, α_{max} represents the maximum ground acceleration (PGA), g is the acceleration due to gravity, σ_{vo} and σ'_{vo} are the total and effective overburden stresses and r_d is the stress reduction coefficient. The value of r_d is calculated using the depth-dependent shear stress reduction equations proposed by Seed and Idriss [26] as follows:

$$\begin{gathered} r_d = 1 - 0.00765z, \text{for } z \leq 9.15\ m \\ r_d = 1.174 - 0.0267z, \text{for } 9.15\ m < z \leq 23\ m \end{gathered} \tag{3.7}$$

Finally, the factor of safety (F_S) against liquefaction is calculated as follows, according to Youd and Idriss [39]:

$$F_S = \frac{CRR_{7.5}}{CSR} MSF \tag{3.8}$$

The magnitude scaling factor (MSF), introduced by Youd and Idriss [39], is estimated using:

$$MSF = \frac{10^{2.24}}{M_w^{2.56}} \tag{3.9}$$

According to the equations provided above, liquefaction is likely to occur when the factor of safety (F_S) at soil layers up to a depth of 20 m from the ground surface is less than 1.0 [26]. Furthermore, it is suggested that liquefaction may still take place even if the F_S is between 1.0 and 1.2 [41, 42].

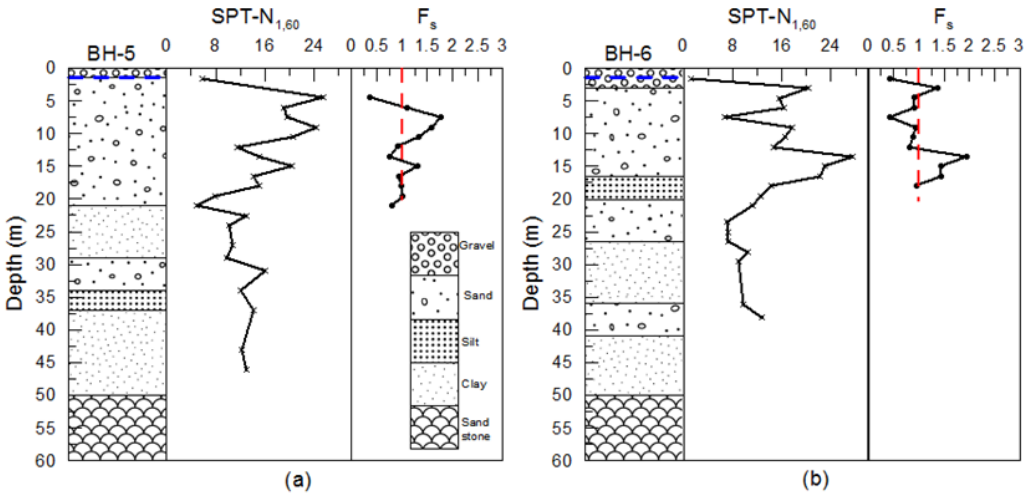

Figure 7. Soil layers at the BH-5, BH-6, BH-7, and BH-8 and corresponding corrected SPT-N values ($N_{1,60}$) and factor of safety (F_S) against liquefaction

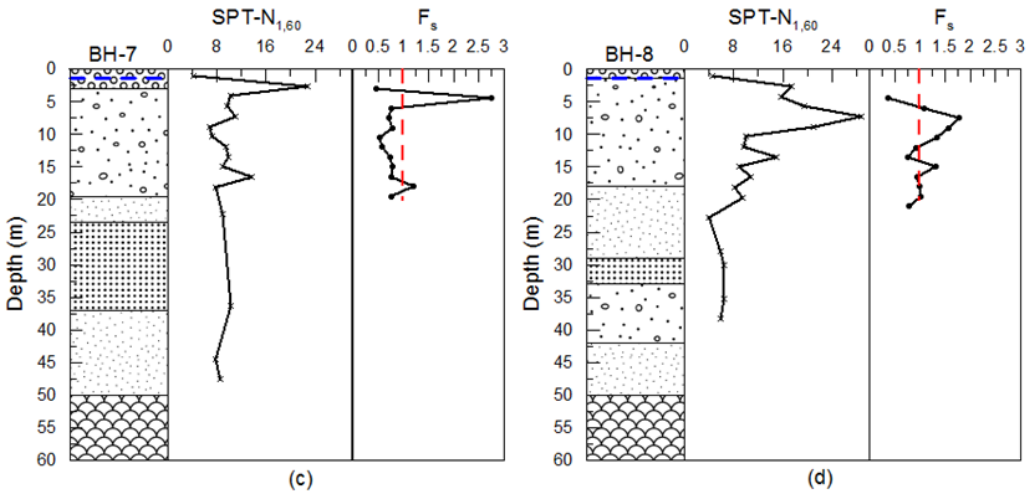

Figure 7. **(Continued)** Soil layers at the BH-5, BH-6, BH-7, and BH-8 and corresponding corrected SPT-N values ($N_{1,60}$) and factor of safety (F_S) against liquefaction

Based on the equations given above, the F_S values at the top 20 m under the PGA of 0.168g (which corresponds to the PGA of the recorded input motion at the #3116 station, as stated in the previous section) are calculated. It is evident that at all the boreholes investigated, F_S values fall below 1, as illustrated in Figures 6-8. Even though the applied PGA (i.e., 0.168g) is well lower than the one suggested by AFAD (i.e., on average 0.35g), liquefaction appears to occur at most of the 20 m. This can be attributed to the fact that the top 20 m consists mostly of sandy soil and $N_{1,60}$ values are quite low, which initiates liquefaction.

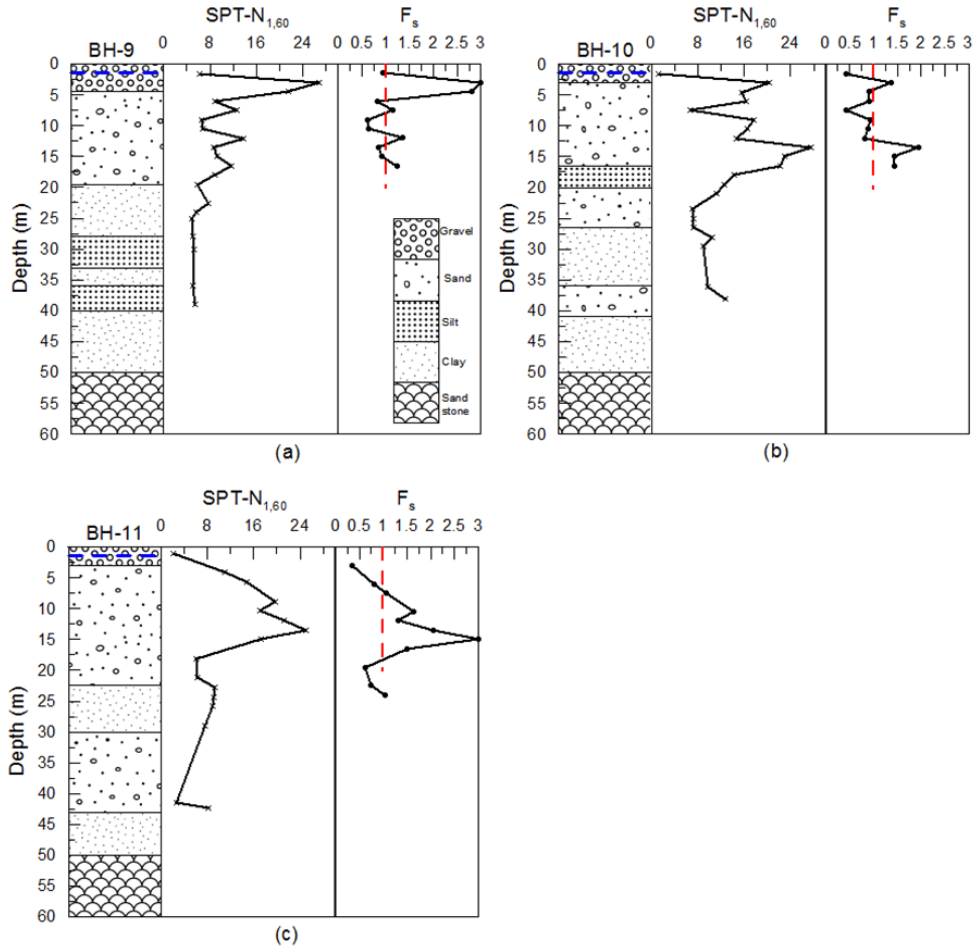

Figure 8. Soil layers at the BH-9, BH-10, and BH-11 and corresponding corrected SPT-N values $(N_{1,60})$ and factors of safety (F_S) against liquefaction

4. Numerical Modelling and Liquefaction Analysis

4.1. Details of the Numerical Modelling

In this study, the liquefaction at the site is also assessed through a numerical approach. For this purpose, the recorded input motion during the Kahramanmaraş earthquake event at the #3116 station is utilized. The acceleration-time history of the input motion in the EW direction is adapted, as already presented in Section 2. The reason for selecting the recording at the #3116 station is that it is located on top of a rock, as such the bottom of the numerical model is considered. Since the aim here is to illustrate the performance of the numerical approach in predicting liquefaction (i.e., accumulation of excess pore water pressure), only the two soil profiles (BH-1 and BH-9) are modeled and simulated.

The numerical analysis is conducted using the open-source finite element software OpenSees [43]. The behavior of sandy soil layers is modeled using a pressure-dependent multi-yield surface constitutive model (PDMY) [44], while the clay soil layers are modeled with a pressure-independent multi-yield surface constitutive model (PIDMY), developed by Gu et al. [45]. The PDMY model simulates elastic-plastic behavior, capturing dilatancy and non-flow liquefaction (cyclic mobility) in sandy and silty soils under the dynamic loading. Its plasticity follows a non-associative flow rule with Drucker-Prager-type multi-yield surfaces. The PIDMY model, on the other hand, is an elastic-plastic model where plasticity is observed only in the deviatoric stress-strain response, while the volumetric stress-strain response is linear-elastic and independent of deviatoric behavior. Its plasticity follows an associative flow rule with Von Mises-type multi-yield surfaces, making it suitable for simulating the monotonic or cyclic material responses where the shear behavior is unaffected by the changes in confinement, such as in organic soils or clay under rapid undrained loading.

No experimental cyclic test data is available for the soil in the study area, preventing direct calibration of the soil model parameters. However, parameters like saturated soil mass density, reference shear and bulk moduli, friction angle, cohesion, and Poisson's ratio are known (see Table 3). Other parameters, including phase transformation angle and liquefaction parameters, are adjusted based on Rahmani et al. [46].

Table 3. PDMY and PIDMY model parameters for different soil layers at BH-1

	BH-1			
	PDMY model parameters			**PIDMY model parameters**
	0-15 m gravel and sand layers	**15-19.5 m silt layer**	**33-42 m gravel and sand layer**	**19.5-33 m and 42-50 m clay layers**
Saturated soil mass density (t/m^3)	1.98	1.95	1.98	1.8
Reference shear modulus (MPa)	70.85	62.93	53.46	53.34
References bulk modulus (MPa)	118	104.88	71.288	71.288
Reference mean effective confining pressure (kPa)	80	80	80	80
Friction angle (degree)	37	25	38	0
Cohesion (kPa)	Not applicable	Not applicable	Not applicable	40
Phase transformation angle (degree)	26	26	26	Not applicable
Peak shear strain (at $p'_r = 80$ kPa)	0.1	0.1	0.1	0.1
Pressure-dependent coefficient	0.13	0.13	0.13	Not applicable
Contraction rate constant	0.13	0.13	0.13	Not applicable
Dilation rate constant 1	0.06	0.06	0.06	Not applicable
Dilation rate constant 2	3	3	3	Not applicable
Liquefaction parameter 1 (kPa)	10	10	10	Not applicable
Liquefaction parameter 2 (kPa)	0.02	0.02	0.02	Not applicable
Liquefaction parameter 3 (kPa)	1	1	1	Not applicable
Permeability (cm/s)	2.5e-4	2.5e-4	2.5e-4	1e-4
Poisson's ratio	0.27	0.27	0.27	Not applicable

Table 4. PDMY and PIDMY model parameters for different soil layers at BH-9

	BH-9			
	PDMY model parameters			**PIDMY model parameters**
	0-19.5 m gravel and sand layers	**28-33 m silt layer**	**36-40 m gravel and sand layer**	**19.5-28 m, 33-36 m and 42-50 m clay layers**
Saturated soil mass density (t/m^3)	1.98	1.95	1.98	1.8
Reference shear modulus (MPa)	74.30	55.64	56.63	58.1
References bulk modulus (MPa)	123.58	92.73	94.387	96.8
Reference mean effective confining pressure (kPa)	80	80	80	80
Friction angle (degree)	38	25	38	8.8
Cohesion (kPa)	Not applicable	Not applicable	Not applicable	28
Phase transformation angle (degree)	26	26	26	Not applicable
Peak shear strain (at $p_r' = 80$ kPa)	0.1	0.1	0.1	0.1
Pressure-dependent coefficient	0.13	0.13	0.13	Not applicable
Contraction rate constant	0.13	0.13	0.13	Not applicable
Dilation rate constant 1	0.06	0.06	0.06	Not applicable
Dilation rate constant 2	3	3	3	Not applicable
Liquefaction parameter 1 (kPa)	10	10	10	Not applicable
Liquefaction parameter 2 (kPa)	0.02	0.02	0.02	Not applicable
Liquefaction parameter 3 (kPa)	1	1	1	Not applicable
Permeability (cm/s)	2.5e-4	2.5e-4	2.5e-4	1e-4
Poisson's ratio	0.27	0.27	0.27	Not applicable

The soil models are formed by nine-node quadrilateral elements, where corner nodes have three degrees of freedom (two translational and one pore pressure), while interior nodes have two translational degrees of freedom. Material properties from Table 5 are assigned to these elements, and only vertical body forces (gravitational acceleration) are considered. The saturated soil model is a two-phase material based on Biot's theory [47] for porous media, considering interactions between the solid and fluid phases simultaneously [48].

The 50 m deep soil models are meshed with elements 2 m wide and 0.5 m high, resulting in 100 elements and 603 nodes. This mesh configuration ensures the minimum node distance, which should be within one-tenth to one-eighth of the seismic wavelength [49]. Periodic boundary conditions are applied to the model sides, guaranteeing equal displacements for nodes with identical vertical coordinates. The bottom nodes are fixed for vertical movement. The underlying elastic medium is modeled with a Lysmer and Kuhlemeyer [50] dashpot connected to the soil model at the bottom node where the dynamic motion is applied. Both the dashpot and the soil model nodes share the same degrees of freedom. To dissipate earthquake energy at the low strain levels, 2% Rayleigh damping (system damping) is used [51].

4.2. Results of Numerical Liquefaction Analysis

The numerical analyses are conducted at only two boreholes (i.e., BH-1 and BH-9) under the recorded input motion at Station #3116. The station is positioned on rock, and the input motion of the first main Kahramanmaraş earthquake event in the EW direction, presented in Section 2, is utilized during the analyses. The excess pore water pressure ratios (r_u), which is the ratio of residual pore water pressure to the effective stress during the dynamic movement of the soil body, are plotted at different depths. Primarily, the r_u values are presented at depths of 7.5 m, 10 m, 15 m, 30 m, 37.5 m, and 45 m.

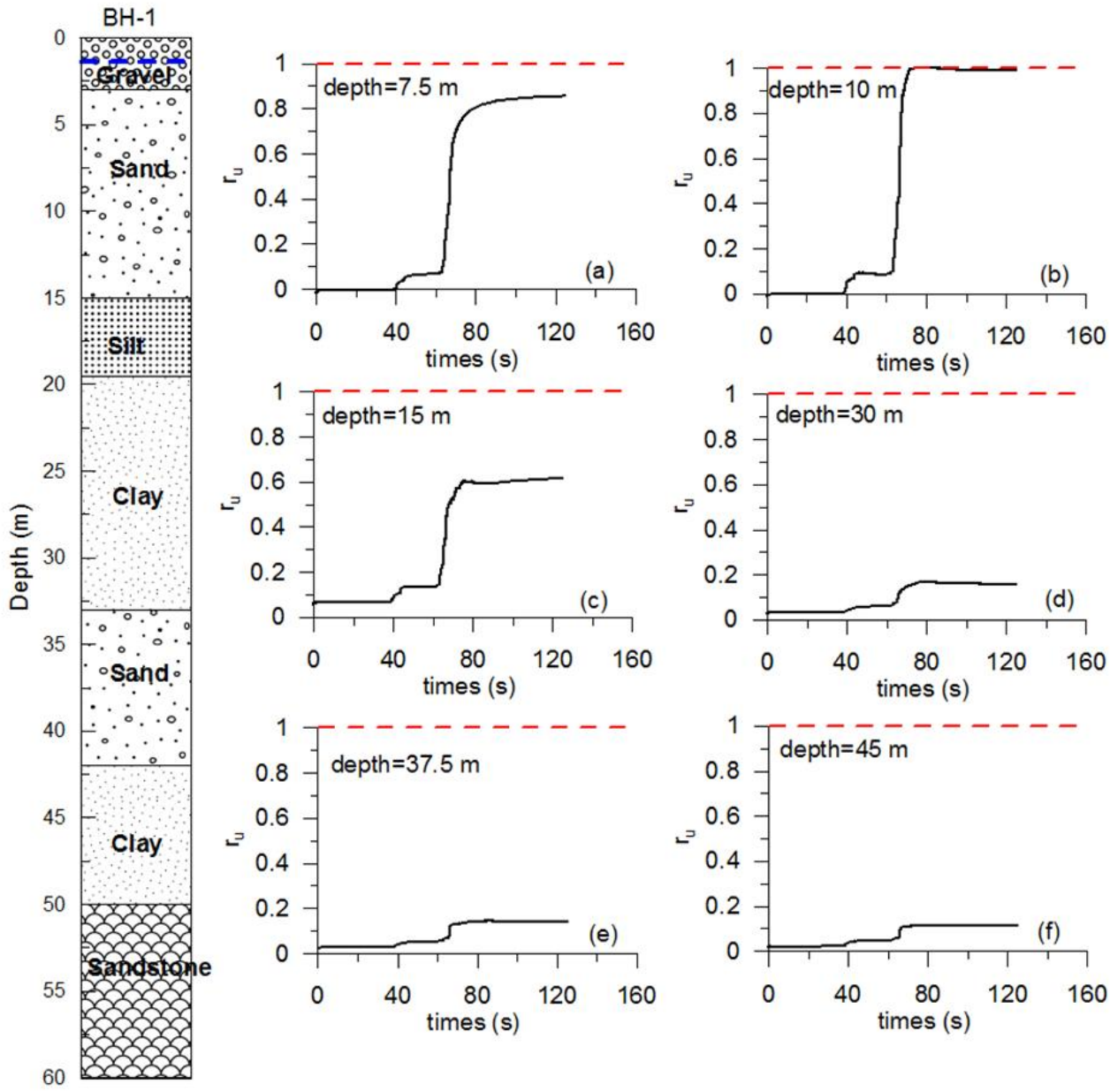

Figure 9. The excess pore water pressure ratios at different depths of BH-1 under the input motion from the first main Kahramanmaraş earthquake event

The r_u values are well below the critical threshold value of 1.0 at depths below 20 m of both boreholes (Figures 9 and 10). In particular, at the BH-1, the built-up excess pore water pressure ratio reaches its maximum values of 0.115, 0.143, and 0.167 at depths of 45 m, 37.5 m, and 30 m, respectively. The maximum r_u values at the same depths of BH-9 are 0.118, 0.141, and 0.185, respectively. However, the r_u values increase above the 20 m depths as the pore water pressure accumulates further progressively. This can be clearly observed in Figures 9a, 9b, and 9c, as well as in Figures 10a, 10b, and 10c. The maximum r_u value rises to 0.614 at the depth of 15 meters in BH-1. Moreover, at the depth of 10 m in the same borehole, liquefaction is likely to occur as the r_u reaches 1.0 (Figure 9b). In contrast, the r_u value reduces to 0.855 at the depth of 7.5 m, as illustrated in Figure 9a. Similarly, the r_u prediction from the numerical analysis indicates liquefaction potential at around the 10 m depth in BH-9, with its value almost reaching 1.0 (i.e., 0.98) (Figure 10b). At depths of 7.5 m and 15.5 m in the BH-9, the maximum r_u values are predicted to be 0.97 and 0.35, respectively.

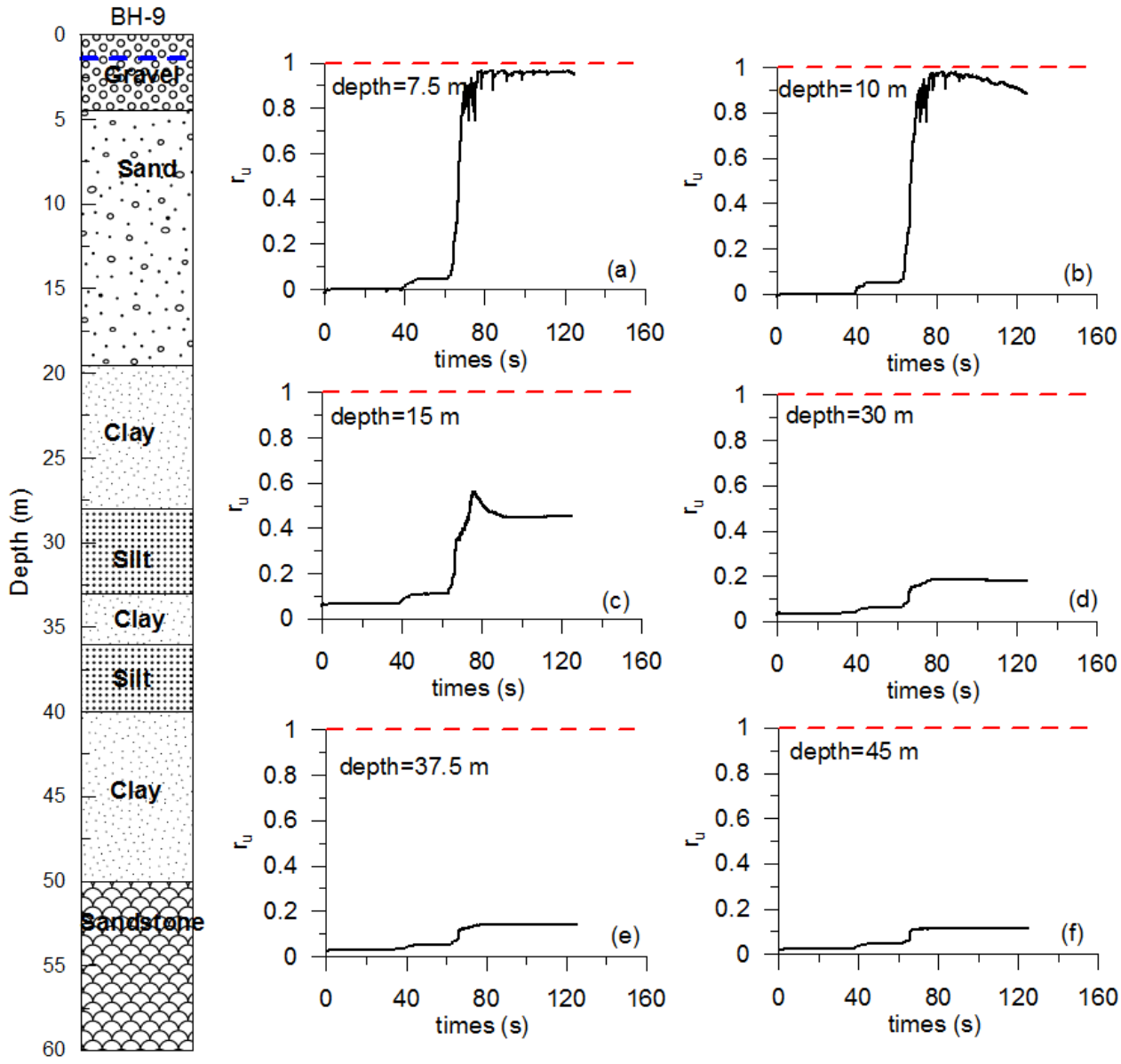

Figure 10. The excess pore water pressure ratios at different depths of BH-9 under the input motion from the first main Kahramanmaraş earthquake event

5. Conclusions

This study focuses on predicting liquefaction cases at a site near the Iskenderun Bay, as observed during the first major earthquake event in Kahramanmaraş on February 6th, 2023. For this, the soil features at 11 boreholes that are drilled for site investigation around the Iskenderun Bay are considered. From the boreholes, mainly, the SPT-N values, soil classification, fine content, and water table are extracted. For predicting the actual liquefaction case, both simplified and numerical methods are considered. The recorded input motion of the earthquake event around the site (at the #3116 station positioned on rock) is considered. The PGA of the recorded input motion is 0.168g. The outcomes of the research presented can be listed as follows:

i. As the top 20 m of the investigated site is characterized by sandy soil with low stiffness (with SPT-N values between 8 to 15, on average), both simplified and numerical methods predict the liquefaction under the PGA of 0.168g,

ii. The numerical analyses demonstrate the increase of excess pore water pressure ratio (r_u) towards the ground surface, especially between 5 to 15 m depths,

iii. The advantage of numerical analyses explicitly indicating the built-up of excess pore water pressure is expressed,
iv. Both the simplified and numerical methods appear to predict liquefaction accurately.

Overall, the liquefaction case at the site close to the Iskenderun Bay is well estimated by both the simplified and numerical methods. Therefore, the assessment of liquefaction potential by these methods is feasible. Nevertheless, the use of a nonlinear numerical method may be appreciated more as it captures the accumulation of excess pore water pressure and, therefore, the stiffness loss. For future work, the soil models will be analyzed along with the building models, allowing for the observation of building responses under the liquefied soil layers. Additionally, triaxial cyclic tests will be conducted to verify the liquefaction cases experimentally.

Author Contributions

The authors read and approved the final version of the paper. All authors contributed equally to this work. They all read and approved the final version of the paper.

Conflict of Interest

All the authors declare no conflict of interest.

Ethical Review and Approval

No approval from the Board of Ethics is required.

References

[1] S. L. Kramer, Geotechnical earthquake engineering, Pearson Education India, 1996.

[2] Y. Zhang, Y. Xie, Y. Zhang, J. Qiu, S. Wu, *The adoption of deep neural network (DNN) to the prediction of soil liquefaction based on shear wave velocity*, Journal of Bulletin of Engineering Geology and the Environment 80 (6) (2021) 5053-5060.

[3] C. Meisina, R. Bonì, F. Bozzoni, D. Conca, C. Perotti, P. Persichillo, C. G. Lai, *Mapping soil liquefaction susceptibility across Europe using the analytic hierarchy process*, Bulletin of Earthquake Engineering 20 (11) (2022) 5601-5632.

[4] S. Lirer, A. Chiaradonna, L. Mele, *Soil liquefaction: From mechanisms to effects on the built environment*, Italian Geotechnical Journal-Rivista Italiana Di Geotecnica 54 (3) (2020) 23-51.

[5] M. Kazama, N. Sento, R. Uzuoka, M. Ishimaru, *Progressive damage simulation of foundation pile of the Showa bridge caused by lateral spreading during the 1964 Niigata earthquake*, presented at the 2nd International Conference for Disaster Mitigation and Rehabilitation, Nanjing, CHINA, May 30-Jun 02, 2008.

[6] S. Bhattacharya, K. Tokimatsu, K. Goda, R. Sarkar, M. Shadlou, M. Rouholamin, *Collapse of Showa Bridge during 1964 Niigata earthquake: A quantitative reappraisal on the failure mechanisms*, Soil Dynamics and Earthquake Engineering 65 (2014) 55-71.

[7] A. Chiaradonna, A. d'Onofrio, F. Silvestri, G. Tropeano, *Prediction of nonlinear soil behaviour in saturated sand: A loosely coupled approach for 1D effective stress analysis*, presented at the 7th International Conference on Earthquake Geotechnical Engineering (ICEGE), Rome, ITALY, Jun 17-20, 2019.

[8] Y. B. Sönmezer, A. Akyüz, K. Kayabali, *Investigation of the effect of grain size on liquefaction potential of sands*, Geomechanics and Engineering 20 (3) (2020) 243-254.

[9] A. Isik, N. Unsal, A. Gurbuz, E. Sisman, *Assessment of liquefaction potential of Fethiye based on spt and shear wave velocity*, Journal of the Faculty of Engineering and Architecture of Gazi University 31(4) (2016) 1027-1037.

[10] R. Ulusay, T. Kuru, *1998 Adana-Ceyhan (Turkey) earthquake and a preliminary microzonation based on liquefaction potential for Ceyhan town*, Natural Hazards 32 (1) (2004) 59-88.

[11] B. Sonmez, R. Ulusay, *Liquefaction potential at Izmit Bay: comparison of predicted and observed soil liquefaction during the Kocaeli earthquake*, Bulletin of Engineering Geology and the Environment 67 (1) (2008) 1-9.

[12] M. Cubrinovski, R. Green, J. Allen, S. Ashford, E. Bowman, B. Bradley, B. Cox, T. Hutchinson, E. Kavazanjian, R. Orense, M. Pender, M. Quigley, L. Wotherspoon, *Geotechnical reconnaissance of the 2010 Darfield (Canterbury) earthquake*, Bulletin of the New Zealand Society for Earthquake Engineering 43 (4) (2010) 243.

[13] B. W. Maurer, R. A. Green, M. Cubrinovski, B. A. Bradley, *Evaluation of the liquefaction potential index for assessing liquefaction hazard in Christchurch, New Zealand*, Journal of Geotechnical and Geoenvironmental Engineering 140 (7) (2014) 04014032.

[14] S. Sassa, T. Takagawa, *Liquefied gravity flow-induced tsunami: first evidence and comparison from the 2018 Indonesia Sulawesi earthquake and tsunami disasters*, Landslides 16 (1) (2019) 195-200.

[15] T. Görüm, H. Tanyas, F. Karabacak, A. Yılmaz, S. Girgin, K. E. Allstadt, M. L. Süzen, P. Burgi, *Preliminary documentation of coseismic ground failure triggered by the February 6th, 2023 Türkiye earthquake sequence*, Engineering Geology Article 327 (2023) 107315.

[16] Y. Guzel, *The 06.02.2023 Kahramanmaraş (Türkiye) earthquake events: The characteristics of the recorded input motions at different sites and their effect on structures*, Journal of Earthquake Engineering (2024) 1-28.

[17] A. Demir, E. Celebi, H. Ozturk, Z. Ozcan, A. Ozocak, E. Bol, S. Sert, F. Z. Sahin, E. Arslan, Z. D. Yaman, M. Utkucu, N. Mert., *Destructive impact of successive high magnitude earthquakes occurred in Türkiye's Kahramanmaraş on February 6th, 2023*, Bulletin of Earthquake Engineering (Special issue) (2024).

[18] H. Ünal, Z. A. Ergüler, *The effect of Kahramanmaraş earthquakes on engineering structures in Adıyaman-Gölbaşı settlement area and earthquake-soil interaction*, Yerbilimleri/ Earth Sciences Article 44 (2023) 202-221, 1313819.

[19] E. Vuran, C. Serhatoglu, M. Timuragaoglu, E. Smyrou, I. E. Bal, R. Livaoglu, *Damage observations of RC buildings from 2023 Kahramanmaraş earthquake sequence and discussion on the seismic code regulations*, Bulletin of Earthquake Engineering (2024).

[20] E. Cakir, K. O. Cetin, *Liquefaction triggering and induced ground deformations at a metallurgical facility in Dörtyol-Hatay after the February 6th Kahramanmaraş earthquake sequence*, Soil Dynamics and Earthquake Engineering Article 178 (2024) 108465.

[21] P. Ozener, M. M. Monkul, E. E. Bayat, A. Ari, K. O. Cetin, *Liquefaction and performance of foundation systems in Iskenderun during 2023 Kahramanmaras-Turkiye earthquake sequence*, Soil Dynamics and Earthquake Engineering 178 (2024) 108433.

[22] J. F. Bird, J. J. Bommer, *Earthquake losses due to ground failure*, Engineering Geology 75 (2) (2004) 147-179.

[23] A. Khosravifar, A. Elgamal, J. Lu, J. Li, *A 3D model for earthquake-induced liquefaction triggering and post-liquefaction response*, Soil Dynamics and Earthquake Engineering 110 (2018) 43-52.

[24] Ö. Yıldız, A. Zeybek, Y. B. Sönmezer, *Investigation of the earthquake-induced liquefaction and seismic amplification after Pazarcık (Mw 7.7) and Elbistan (Mw 7.6) earthquakes*, Environmental Earth Sciences 83 (21) (2024) 1-21.

[25] K. O. Cetin, B. Soylemez, H. Guzel, E. Cakir, *Soil liquefaction sites following the February 6th, 2023, Kahramanmaraş-Türkiye earthquake sequence*, Bulletin of Earthquake Engineering (Special issue) (2024).

[26] H. B. Seed, I. M. Idriss, *Simplified procedure for evaluating soil liquefaction potential*, ASCE Journal of Soil Mechanics and Foundations Division 97 (SM9) (1971) 1249-1273.

[27] Y. Guzel, M. A. Ozdemir, *Liquefaction hazard assessments in Igdır city (Turkey)*, Erciyes University Journal of Institue Of Science and Technology 40 (1) (2024) 148-166.

[28] W. Zhang, Y. Dong, J. G. F. Crempien, P. Arduino, A. Kurtulus, E. Taciroglu, *A comparison of ground motions predicted through one-dimensional site response analyses and three-dimensional wave propagation simulations at regional scales*, Earthquake Spectra 40 (2) (2024) 1215-1234.

[29] C. A. de la Torre, B. A. Bradley, F. Kuncar, R. L. Lee, L. M. Wotherspoon, A. E. Kaiser, *Combining observed linear basin amplification factors with 1D nonlinear site-response analyses to predict site response for strong ground motions: Application to Wellington, New Zealand*, Earthquake Spectra 40 (1) (2024) 143-173.

[30] C. Visone, F. S. de Magistris, E. Bilotta, *Comparative study on frequency and time domain analyses for seismic site response*, Electronic Journal of Geotechnical Engineering 15 A (2010) 1-20.

[31] R. Sun, X. Yuan, *A holistic equivalent linear method for site response analysis*, Soil Dynamics and Earthquake Engineering 141 (2021) 106476.

[32] C. Bolisetti, A. S. Whittaker, H. B. Mason, I. Almufti, M. Willford, *Equivalent linear and nonlinear site response analysis for design and risk assessment of safety-related nuclear structures*, Nuclear Engineering and Design 275 (2014) 107-121.

[33] Ö. Yıldız, E. Doğan, *Soil-structure interaction analysis of Çelebiağa Mosque*, Pertek-Türkiye Revista De La Construcción 21 (3) (2022) 750-766.

[34] Y. Guzel, F. Guzel, *Evaluation of EC8 and TBEC design response spectra applied at a region in Turkey*, Earthquakes and Structures 25 (3) (2023) 199-208.

[35] Y. Guzel, F. Guzel, *Investigation of local site effect considering the recordings of the 08.11.2021 earthquake event in Konya, Turkey*, Natural Hazards 116 (1) (2023) 619-636.

[36] Y. Guzel, F. Güzel, *Site response predictions at Atakoy downhole array*, Dokuz Eylul University Faculty of Engineering Journal of Science and Engineering 25 (75) (2023) 739-750.

[37] Y. Guzel, *Site response analyses with different stiffness profiles and input motion variability*, Geotechnical and Geological Engineering 42 (3) (2024) 2075-2091.

[38] H. B. Seed, K. Tokimatsu, L. F. Harder, R. M. Chung, *Influence of SPT procedures in soil liquefaction resistance evaluations*, Journal of Geotechnical Engineering-ASCE 111 (12) (1985) 1425-1445.

[39] T. L. Youd, I. M. Idriss, *Liquefaction resistance of soils: Summary report from the 1996 NCEER and 1998 NCEER/NSF workshops on evaluation of liquefaction resistance of soils*, Journal of Geotechnical and Geoenvironmental Engineering 127 (4) (2001) 297-313.

[40] S. S. C. Liao, R. V. Whitman, *Overburden correction factors for SPT in sand*, Journal of Geotechnical Engineering-ASCE 112 (3) (1986) 373-377.

[41] H. Tosun, R. Ulusay, *Engineering geological characterization and evaluation of liquefaction susceptibility of foundation soils at a dam site, southwest Turkey*, Environmental & Engineering Geoscience 3 (3) (1997) 389-409.

[42] E. S. Duman, S. B. Ikizler, Z. Angin, *Evaluation of soil liquefaction potential index based on SPT data in Erzincan, Eastern Turkey,* Arabian Journal of Geosciences 8 (7) (2015) 5269-5283.

[43] S. Mazzoni, F. McKenna, M. H. Scott, G. L. Fenves, Open system for earthquake engineering simulation user manual, Ed. Berkeley Calif: University of California, 2009.

[44] Z. Yang, *Numerical modeling of earthquake site response including dilation and liquefaction*, PhD dissertation, Dept. of Civil Engineering and Engineering Mechanics, Columbia University (2000), Columbia.

[45] Q. Gu, J. P. Conte, Z. Yang, A. Elgamal, *Consistent tangent moduli for multi-yield-surface J 2 plasticity model*, Computational Mechanics 48 (2011) 97-120.

[46] F. Rahmani, S. M. Hosseini, A. Khezri, M. Maleki, *Effect of grid-form deep soil mixing on the liquefaction-induced foundation settlement, using numerical approach*, Arabian Journal of Geosciences 15 (12) (2022) 1112.

[47] M. A. Biot, *The mechanics of deformation and acoustic propagation in porous media*, Journal of Applied Physics 33 (1482) (1962).

[48] O. C. Zienkiewicz, A. H. C. Chan, M. Pastor, D. K. Paul, T. Shiomi, *Static and dynamic behavior of soils: a rational approach to quantitative solutions: I. Fully saturated problems*, Proceedings of the Royal Society a Mathematical, Physical and Engineering Sciences 429 (1990).

[49] K. J. Bathe, Finite element procedures in engineering analysis. Upper Saddle River, NJ: Prentice, 1982.

[50] J. Lysmer, R. L. Kuhlemeyer, *Finite dynamic model for infinite media*, Journal of the Engineering Mechanics Division 95 (1969).

[51] R. W. Clough, J. Penzien, Dynamics of structures, Berkeley: Computers and Structures, Inc., 2003.